IOP Publishing Measurement Science and Technology
Meas. Sci. Technol. **31** (2020) 045201 (8pp) https://doi.org/10.1088/1361-6501/ab501a

High-precision frequency sweeping interferometry for absolute distance measurement using a tunable laser with sweeping range of 88 GHz

Guang Shi[1,2,3], **Kefei Hei**[2], **Wen Wang**[1] and **Nandini Bhattacharya**[2]

[1] School of Mechanical Engineering, Hangzhou Dianzi University, No. 1158 the No. 2 Street, Hangzhou 310018, People's Republic of China
[2] Optics Research Group, Department of Applied Sciences, Technical University Delft, Lorentzweg 1, 2628 CJ Delft, The Netherlands

E-mail: shiguang@hdu.edu.cn

Received 15 July 2019, revised 19 October 2019
Accepted for publication 22 October 2019
Published 6 January 2020

Abstract

Distance measurement using frequency sweeping interferometry is an absolute distance measurement technique that allows for high accuracy over long distances. Notwithstanding, the measurement accuracy is affected by laser sweeping nonlinearity and limited sweeping range. In this work, an optimized post-processing linearization method is demonstrated to realize high-accuracy arbitrary distance measurement using a laser with small modulation range. The interference signal is sparsely resampled to eliminate the influence of the sweeping nonlinearity, and the absolute distance is obtained by analyzing the phase of the resampled signal. In the measurement system, a high-finesse Fabry–Pérot cavity placed in vacuum is used as the measurement reference, so the effect of dispersion mismatch is negligible. Moreover, the distance measurement result is determined by the linear fit of the phase of each resampled point. Therefore, the influence of target vibration and other external random noise can be partially eliminated, and the reliability of the result is high. In the experiment, the sweeping range of the laser source is only 88 GHz. Comparing with a fringe-counting interferometer, the standard deviation of the residual errors is 34 μm within a distance of 6.7 m.

Keywords: laser distance measurement, absolute distance measurement, frequency sweeping interferometry

(Some figures may appear in colour only in the online journal)

1. Introduction

High-accuracy and precision-absolute distance measurement is vital to large-scale manufacturing [1, 2], tight-formation flying of satellites [2] and autonomous driving [3]. Distance measurement using frequency sweeping interferometry (FSI) is a promising method because of its high accuracy at long ranges. Compared with absolute distance measurement systems based on optical frequency combs [4] and high-frequency RF systems [5], FSI systems have the characteristics of simple structure and low cost.

For a distance measurement system based on FSI, the measured distance L can be estimated by $L = c\Delta\Phi/(2\pi \cdot B \cdot n_g)$, where B is the optical frequency sweeping range of the laser, $\Delta\Phi$ is the phase change of the interference signal, c is the speed of light in vacuum and n_g is the group refractive index of air [6, 7]. The theoretical measurement accuracy and precision are subject to the sweeping range and linearity of the laser source [8]. There are two main signal processing methods to reduce the impact of these two factors on measurement

[3] Author to whom any correspondence should be addressed.

accuracy and precision. Each of the two methods has advantages and disadvantages.

For the first method, Fabry–Pérot (F–P) cavities are generally used to calculate the optical frequency sweeping range B, and the measurement precision can be easily less than 100 kHz. The measurement of $\Delta\Phi$ depends on the measurement of the intensity of the interference signal. Also, because the frequency of the interference signal varies over time, it is difficult to realize the high-precision measurement of $\Delta\Phi$. This would also lead to the measurement uncertainty of $\Delta\Phi$ being amplified by a large factor. As an example, for a sweep of 50 GHz in a 600 nm wavelength laser, the amplification factor is about 10 000 [9]. Hence, a major contributor to the final measurement uncertainty arises from the imprecision of $\Delta\Phi$. The nonlinearity of the optical frequency sweeping and the vibration of the target will seriously affect the measurement accuracy of $\Delta\Phi$. Adding a compensation system into the instrument can reduce the effect of target vibration, but this increases the complexity of the instrument [10]. Eliminating the effect of target vibration without increasing complexity is also a worthwhile topic to investigate. Kalman filter techniques are also proposed to compensate the measurement errors caused by low-frequency vibration of the target [11–13] and the sweeping nonlinearity of the laser [14]. However, for random vibration of the target, this method would not be very appropriate.

A second method, known as the frequency-sampling method, is a recognized post-processing scheme. In 2011, Baumann *et al* used a femtosecond optical frequency comb as an optical frequency standard to resample the interference signal at equal frequency steps [15, 16], and demonstrated a precision of 10 μm at a distance of 10.5 m. A fiber Mach–Zehnder interferometer is a more cost-effective choice in the frequency-sampling method [17] instead of an optical frequency comb. Pan *et al* added an hydrogen cyanide (HCN) cavity to the laser distance measurement system and used a multiple signal classification (MUSIC) algorithm to enhance the measurement precision to 45 μm within 8 m [18]. Lu *et al* added a laser Doppler velocimetry (LDV) component to the measurement system to compensate for the environmental vibration. A measurement uncertainty of 8.6 μm + 0.16 μm m^{-1} · L ($k = 2$) with a measuring range from 1 m to 24 m was achieved [19]. In order to satisfy the Nyquist sampling theorem, the optical path difference of the Mach–Zehnder interferometer should be at least twice that of the measuring interferometer. The increase in measuring range necessitates that the length of the optical fiber must be increased accordingly, resulting in the effects of fiber jitter [20] and dispersion becoming more significant. Pan [21] and Liu [22], proposed different algorithms to eliminate the dispersion mismatch.

In this paper, we propose an optimized post-processing method and an FSI system for absolute distance measurement with an F–P cavity as the measurement reference. This technique overcomes the shortcomings of the two methods above simultaneously. Compared with a fiber Mach–Zehnder interferometer, the F–P cavity is more stable and traceable; and because the F–P cavity is placed in vacuum, the problem of dispersion mismatch does not exist for the distance measurement system. Although the interference signal is sparsely resampled, arbitrary distance is obtained with only one F–P cavity. The measurement result is determined by a linear fit of the phase of each resampled point. So the influence of target vibration and other external random noise can be partially eliminated, and the reliability of the result is higher than a traditional FSI system. In the experiment, the sweeping range of the tunable laser is only 88 GHz. Comparing with a commercial fringe-counting interferometer, a standard deviation of the residual errors of 34 μm with a measuring range from 2200 mm to 6700 mm has been shown.

2. Methodology

The distance measurement technique we propose and demonstrate in this work is based on FSI. An external cavity diode laser (ECDL) is used as the optical frequency sweeping laser source, and a F–P cavity is used to generate the periodic maxima to resample the interference signal from the measurement interferometer. This measurement is then compared with a commercial fringe-counting interferometer.

Figure 1 illustrates a schematic of the proposed FSI for absolute distance measurement. This system mainly consists of five parts: a tunable laser source, an F–P interferometer, a measurement Michelson interferometer, a commercial fringe-counting interferometer and a control and DAQ system. Directly after the ECDL and the optical isolator, a few optical components prepare the beam for use in the rest of the setup. After the initial beam-shaping, the light is divided into two paths using a polarizing beam splitter. The half-wave plate placed before the beam splitter can be rotated to vary the splitting ratio between the F–P interferometer and the measurement interferometer. The measurement interferometer is a Michelson interferometer with photodetector 1 (PD1) measuring its output. Similarly, PD2 measures the output of the F–P interferometer.

The beat signal detected by PD1 at the output from the measurement interferometer can be expressed as

$$I(\upsilon) = I_0 \cos(2\pi \cdot D \cdot n \cdot \upsilon/c), \tag{1}$$

where I_0 denotes the amplitude of the interference signal, υ denotes the instantaneous optical frequency, D denotes the optical path difference of the measurement interferometer, n denotes the phase refractive index of air for a wavelength of $\lambda = c/\upsilon$ and c is the velocity of light in vacuum.

Sweeping nonlinearity of the laser results in nonlinearity of υ and time. Thus, the measurement interferometer signal acquired by the DAQ is not a fixed-frequency cosine signal. This is the main reason why the nonlinearity of the laser leads to a decrease of measurement accuracy.

Defining the argument of the cosine of equation (1) as

$$\phi = 2\pi \cdot D \cdot n \cdot \upsilon/c \tag{2}$$

and taking the derivative with respect to frequency, we get

$$\frac{\mathrm{d}\phi}{\mathrm{d}\upsilon} = \frac{2\pi D}{c}\left(n + \upsilon\frac{\mathrm{d}n}{\mathrm{d}\upsilon}\right) = \frac{2\pi D}{c}n_{\mathrm{g}}, \tag{3}$$

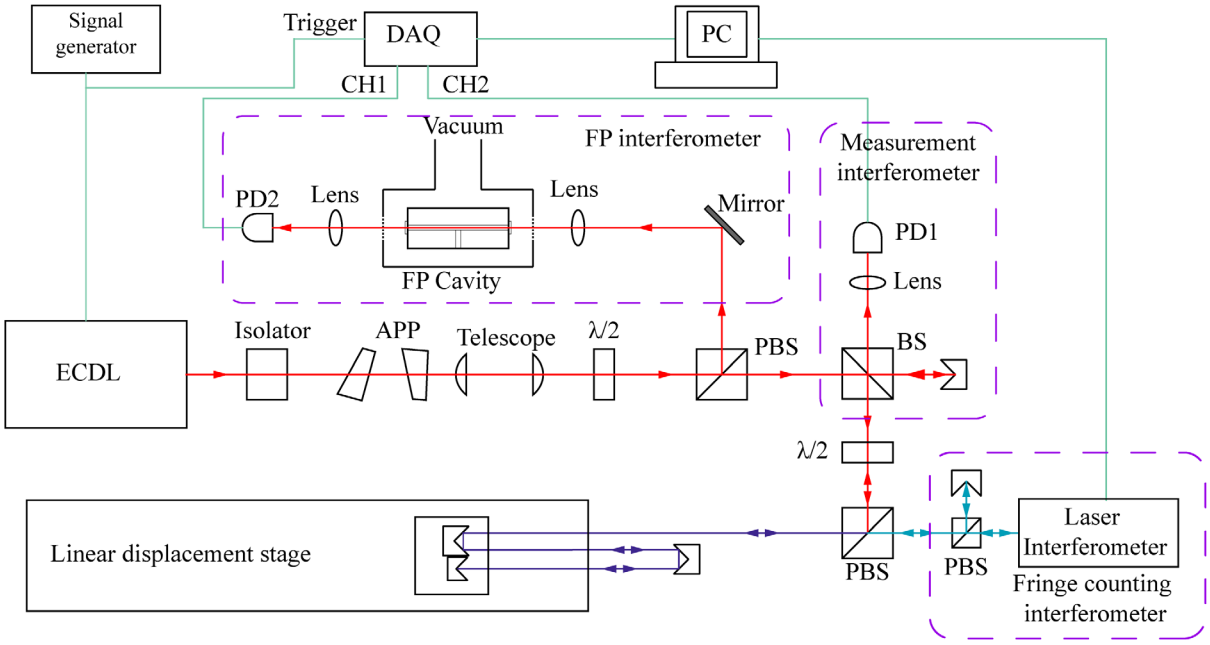

Figure 1. Schematic of the experimental setup of FSI system for absolute distance measurement. ECLD: external cavity laser diode, APP: anamorphic prism pair, BS: beam-splitter, PBS: polarizing beam-splitter, DAQ: data acquisition, PD: photo detector.

where the group refractive index n_g is defined as [23]

$$n_g = n + \upsilon \frac{dn}{d\upsilon}. \tag{4}$$

Then the length to be measured L is only determined from the slope $d\phi/d\upsilon$ [24] as

$$L = \frac{D}{2} = \frac{d\phi}{d\upsilon} \cdot \frac{c}{4\pi n_g}. \tag{5}$$

Since $I(\upsilon)$ represents a function of instantaneous optical frequency υ, if it is resampled with equal optical frequency intervals $\Delta\upsilon$, the effect of laser sweeping nonlinearity will be eliminated. The measurement signal would become

$$\begin{aligned} I(p) &= I_0 \cos\left(\frac{d\phi}{d\upsilon}\Delta\upsilon \cdot p + \phi_0\right) \\ &= I_0 \cos\left(\frac{4\pi \cdot n_g \cdot L \cdot \Delta\upsilon}{c} \cdot p + \frac{4\pi \cdot n_0 \cdot L \cdot \upsilon_0}{c}\right), \end{aligned} \tag{6}$$

where $p = 1, 2, \ldots, N$, and N represents the total number of sampling points, υ_0 denotes the initial optical frequency, n_0 denotes the phase refractive index of the laser with initial optical frequency.

For the F–P interferometer, the difference between two successive resonance frequencies, the free spectral range (FSR) $\Delta\upsilon_{FSR}$ [25] is given by the equation below:

$$\Delta\upsilon_{FSR} = \frac{c}{2 \cdot n \cdot d_{FP}}, \tag{7}$$

where d_{FP} denotes the length of the F–P cavity.

F–P resonance peaks can be used to sample the interference signal with optical frequency intervals equal to the FSR. According to the requirement of the frequency sampling method, the signals of PD1 and PD2 are sampled synchronously. Then, the measurement interference signal could be further sampled at $\Delta\upsilon_{FSR}$, which is calculated as

$$I(i) = I_0 \cos\left(\frac{4\pi \cdot n_g \cdot L \cdot \Delta\upsilon_{FSR}}{c} \cdot i + \frac{4\pi \cdot n_0 \cdot L \cdot \upsilon_0}{c}\right), \tag{8}$$

where $\Delta\upsilon_{FSR}$ denotes the FSR of the F–P cavity, $i = 1, 2, \ldots, N$, and N denotes the total number of sampling points.

Using d_{FP}, the length of the F–P cavity, we can rewrite the above equation as

$$I(i) = I_0 \cos\left(\frac{2\pi \cdot n_g \cdot L}{d_{FP}} \cdot i + \frac{4\pi \cdot n_g \cdot L \cdot \upsilon_0}{c}\right). \tag{9}$$

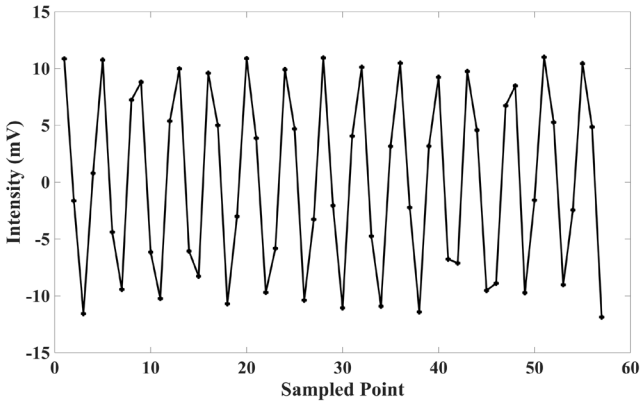

Figure 2. The resampled signal.

Figure 2 shows the resampled signal. We performed a Hilbert transform on the resampled signal to obtain the instantaneous phase. $I(i)$ is the resampled signal of the measurement interference signal. We denote $\tilde{I}(i)$ as the Hilbert transform of $I(i)$. Then the phase of $I(i)$ can be expressed as

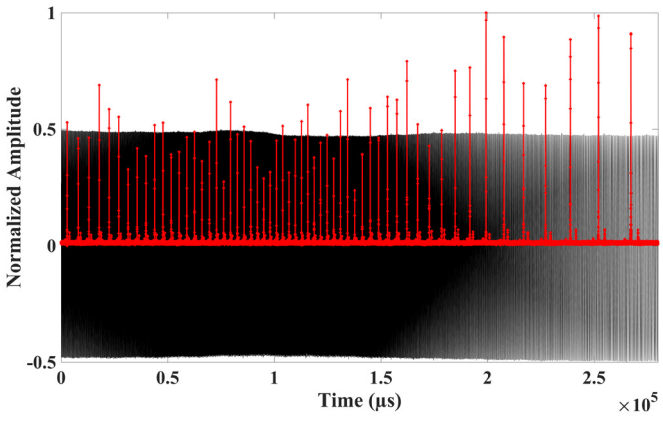

(a)

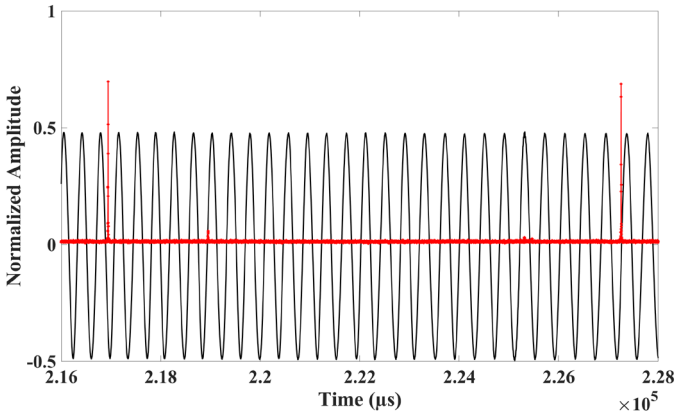

(b)

Figure 3. Interference signal of measurement interferometer (black) and F–P interferometer (red). (a) The signal of one measurement. (b) Enlarged detail of (a) showing fringes between the F–P resonances.

$$\phi(i) = \arctan\frac{I(i)}{\tilde{I}(i)}. \tag{10}$$

After unwrapping the phase $\phi(i)$, we obtain $\phi'(i)$. Then, taking the derivative of $\phi'(i)$ with respect to i, we get the frequency f_I:

$$f_\mathrm{I} = \frac{\mathrm{d}\phi'(i)}{\mathrm{d}i}. \tag{11}$$

f_I is dimensionless and the range is from 0 to 0.5.

The length of the F–P cavity is limited; if the measured distance is larger than the length of the F–P cavity, undersampling would occur, which is shown in figure 3. This leads to an ambiguous measurement result. In order to realize measurement of arbitrary distance, we set M_{ean} as the average number of peaks and valleys of the measurement interferometer signal between every two peaks of the F–P interferometer signal in a single measurement. The absolute distance of the target can be obtained by

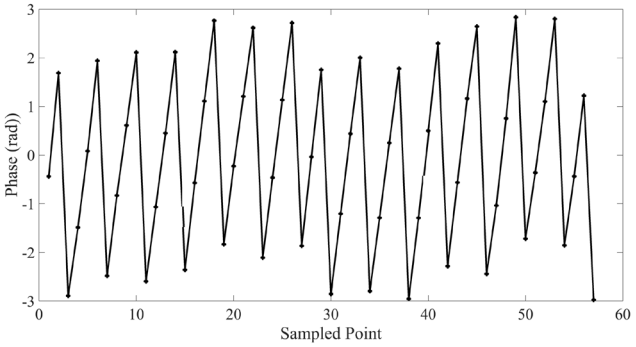

Figure 4. The phase obtained from the Hilbert transform of the resampled signal shown in figure 2.

$$L = \begin{cases} (0.5\cdot m + f_\mathrm{I})\cdot d_{\mathrm{FP}}/n_\mathrm{g} & \text{when } m \text{ is an even number or zero} \\ [0.5\cdot(m+1) - f_\mathrm{I}]\cdot d_{\mathrm{FP}}/n_\mathrm{g} & \text{when } m \text{ is an odd number} \end{cases}, \tag{12}$$

where m is an integer, and $(M_{\mathrm{ean}} - 1) < m\, M_{\mathrm{ean}}$. f_I is the frequency of the resampled interference signal.

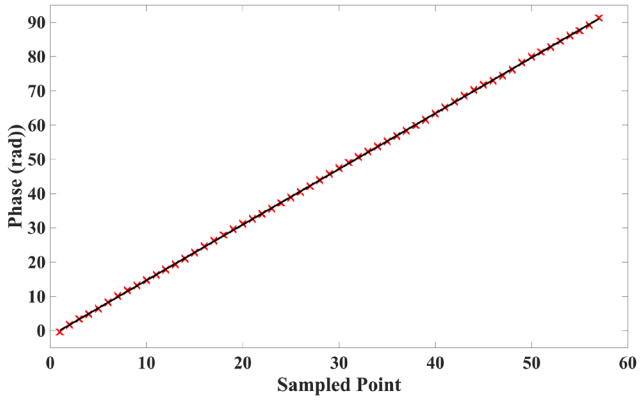

Figure 5. The phase after unwrapping (black) fitted using the least squares function (red).

The uncertainty of the FSI system u_{L} can be obtained from (12) as

$$u_{\mathrm{L}} = \begin{cases} \sqrt{\left(\frac{0.5d_{\mathrm{FP}}}{n_{\mathrm{g}}}\cdot u_{\mathrm{m}}\right)^2 + \left(\frac{0.5m+f_{\mathrm{I}}}{n_{\mathrm{g}}}\cdot u_{d_{\mathrm{FP}}}\right)^2 + \left(\frac{d_{\mathrm{FP}}}{n_{\mathrm{g}}}\cdot u_{f_{\mathrm{I}}}\right)^2 + \left(\frac{0.5\cdot m\cdot d_{\mathrm{FP}}+f_{\mathrm{I}}\cdot d_{\mathrm{FP}}}{n_{\mathrm{g}}^2}\cdot u_{n_{\mathrm{g}}}\right)^2} & \text{when } m \text{ is an even number or zero} \\ \sqrt{\left(\frac{0.5d_{\mathrm{FP}}}{n_{\mathrm{g}}}\cdot u_{\mathrm{m}}\right)^2 + \left(\frac{0.5m+0.5-f_{\mathrm{I}}}{n_{\mathrm{g}}}\cdot u_{d_{\mathrm{FP}}}\right)^2 + \left(\frac{d_{\mathrm{FP}}}{n_{\mathrm{g}}}\cdot u_{f_{\mathrm{I}}}\right)^2 + \left[\frac{0.5\cdot(m+1)\cdot d_{\mathrm{FP}}-f_{\mathrm{I}}\cdot d_{\mathrm{FP}}}{n_{\mathrm{g}}^2}\cdot u_{n_{\mathrm{g}}}\right]^2} & \text{when } m \text{ is an odd number} \end{cases} \tag{13}$$

The major contributor to the final uncertainty is the uncertainty of f_{I} and d_{FP}. Because m is an integer, the uncertainty of m is 0. In the laboratory environment, the uncertainty of n_{g} is small enough to be neglected. Therefore equation (13) can be simplified to

$$u_{\mathrm{L}} = \begin{cases} \sqrt{\left(\frac{0.5m+f_{\mathrm{I}}}{n_{\mathrm{g}}}\cdot u_{d_{\mathrm{FP}}}\right)^2 + \left(\frac{d_{\mathrm{FP}}}{n_{\mathrm{g}}}\cdot u_{f_{\mathrm{I}}}\right)^2} & \text{when } m \text{ is an even number or zero} \\ \sqrt{\left(\frac{0.5m+0.5-f_{\mathrm{I}}}{n_{\mathrm{g}}}\cdot u_{d}\right)^2 + \left(\frac{d_{\mathrm{FP}}}{n_{\mathrm{g}}}\cdot u_{f_{\mathrm{I}}}\right)^2} & \text{when } m \text{ is an odd number} \end{cases}. \tag{14}$$

In our laser distance measurement system, the sweeping range of the ECDL being only 88 GHz, the number of resonances from the F–P cavity which overlap with the measured signal is only 58, which is shown in figure 3. Thus, the length of the resampled signal is only 58 points. Figure 2 shows the resampled signal. We performed a Hilbert transform on the resampled signal to obtain the instantaneous phase, which is shown in figure 4. After unwrapping the phase, we perform a least-squares fit to the phase curve to obtain the fitted curve, as shown in figure 5. The resolved phase is shown in black, and the result of least square fitting of the phase is in red. The slope of the fitted line is 1.625 ± 0.004, with 95% confidence bounds. The frequency of the signal shown in figure 5 is calculated to be $f_{\mathrm{I}} = 0.2586 \pm 0.00064$, again with 95% confidence bounds. Then the group refractive index is $n_{\mathrm{g}} = 1.0002656$, the absolute distance of the target can be calculated for equation (12), $L = (0.5 \times m + f_{\mathrm{I}}) \cdot d_{\mathrm{FP}}/n_{\mathrm{g}} = (0.5 \times 52 + 0.2586) \times 101.768/1.0002656 = 2671.576 \pm 0.065$ mm.

For a traditional FSI system, the measured distance L is estimated by $L = c \cdot \Delta\Phi/(2\pi \cdot B \cdot n_{\mathrm{g}})$. The measurement accuracy is determined by the measurement accuracy of B and $\Delta\Phi$. The measurement of B and $\Delta\Phi$ at the starting and ending positions of laser sweeping greatly affect the reliability of measurement, and the influence of vibration on distance measurement is amplified by a large amplification factor [9]. For our method the result we obtain from figure 5 is determined by all the resampled points, and the measurement error at each point is reduced by averaging. In addition, according to equation (13) the influence of vibration on distance measurement accuracy depends on $(d_{\mathrm{FP}}/n_{\mathrm{g}}) \cdot u_{f\mathrm{I}}$, which is not amplified. Thus the measurement error is not amplified.

3. Experiment

Figure 1 illustrates a schematic diagram of the actual experimental FSI system. In this system, an ECDL (New Focus TLB-6210) is chosen as the tunable laser source with a central wavelength of 633 nm, and the sweeping range available is 88 GHz. The anamorphic prism pair and the telescope are employed to change the elliptical beam cross-section of the laser diode into a circular one, and to improve the collimation of the measurement beam. A signal generator is employed to supply the sweeping signal at the frequency of 2 Hz. The F–P cavity (custom built, Research Electro-Optics; finesse is 11041) is made out of ultra-low expansion (ULE) glass and is placed in vacuum. The free spectral range (FSR) of the F–P cavity was calibrated before the experiment. The length of the FP cavity d_{FP} is calculated by $d_{\mathrm{FP}} = c/2n \cdot \mathrm{FSR} = 101.768$ mm.

The Michelson measurement interferometer is an unbalanced interferometer built with 1-inch-sized optics, using a non-polarizing beam splitter (BS) and retroreflector prisms, whose long arm is used as the length to be measured. The measurement arm has a maximum length of 1.5 m and consists of a long rail with an electric carriage carrying two retroreflector prisms. As is shown in figure 1, the measured optical path is folded three times by three retroreflector prisms. At the nearest measurement position of the rail, the distance difference of the two arms of the measurement interferometer is 2208.877 mm. This position is set to be the measurement origin of the fringe-counting interferometer. A commercial fringe-counting interferometer (Agilent 5519A), with a linear distance measurement accuracy of ± 0.4 ppm in air is used for the comparison measurement.

The beam from the ECLD and the fringe-counting interferometer is combined with a polarizing beam-splitter (PBS). The auxiliary mirrors in the optical path are adjusted to ensure that the two beams overlap optimally. As a result, both beams largely propagate through the same volume of air, having a shared measurement arm. Then the half-wave-plate is

Table 1. Preliminary measurement uncertainty budget according to the Guide to the Expression of Uncertainty in Measurement (GUM).

Quantity	Uncertainty (type A evaluations)	Coverage factor	Standard uncertainty	Sensitivity	Uncertainty contribution
d_{FP}	0.13	2	0.065	21.5–66.0	1.4–4.3 μm
f_I	0.0007	2	0.000 35	101 741.0	35.6 μm
m	0	—	0	50.9	0 μm
n_g	0.000 000 032	2	0.000 000 016	2186.6–6720.3	≈0 μm
Combined standard uncertainty				u_L ($k = 1$)	=35.6–35.9 μm
Combined expanded uncertainty (with coverage factor of $k = 2$)				$u_L(k = 2)$	=71.2–71.8 μm

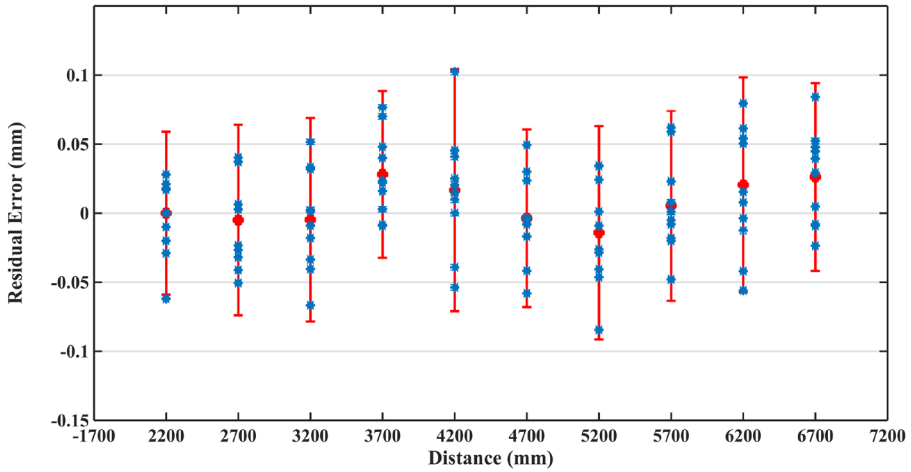

Figure 6. The difference between distance measurement with the FSI system and the fringe-counting interferometer. The red bar denotes twice of the standard deviation of the measurements.

laser from the fringe-counting interferometer propagates back through the same path to the fringe-counting interferometer which contains the detector for fringe counting. The interferometer signal of the Michelson measurement interferometer is detected by PD1. The detected signal of PD1 and PD2 are synchronously sampled by a DAQ board. The bit-width of the DAQ board is 22-bit and the sampling rate is 1 MHz.

In the experiment, the carriage was physically moved from 0 mm to 1500 mm, corresponding to an optical path length of 0 mm to 4500 mm. At each position 10 measurements were made. Moreover, the displacement of the carriage was measured by both the FSI system and the fringe-counting interferometer simultaneously. During the experiment, environmental conditions were measured by a VAISALA air parameter sensor. The temperature, humidity and atmospheric pressure were measured to be 27 ± 0.2 °C, 46.2% ± 0.2% and 101.61 ± 0.02 kPa.

4. Results and discussion

In the experiment, the F–P cavity is located inside a small vacuum vessel and has large thermal mass so the fluctuation in the temperature of the cavity is low. Thus the effect of temperature on the FSR is small enough to be ignored. According to Type A evaluations of uncertainty, the uncertainty of air pressure in the small vacuum vessel is 0.05 kPa. Substituting temperature and humidity parameters, calculating using Edlen's equation, the uncertainty of the refractive index in the F–P cavity is $u_n = 0.000\,000\,13$, the uncertainty of FSR is $u_{FSR} = 180$ Hz. Assuming $n_g = 1$, from equation (7) the uncertainty of physical length of the cavity is $\delta_{d_{FP}} = 0.13$ μm (with coverage factor of $k = 2$). The standard uncertainty of d_{FP} is $u_{d_{FP}} = 0.065$ μm.

The absolute distances obtained from the FSI system vary from about 2200 mm to 6700 mm. The range of m in equations (12) and (13) is from 43 to 131. Table 1 shows the measurement uncertainty budget according to the Guide to the Expression of Uncertainty in Measurement (GUM) [26]. According to Type A evaluations of uncertainty, the measurement uncertainty of resampled frequency f_I is $\delta_{f_I} = 0.0007$ (with coverage factor of $k = 2$). So the standard uncertainty of f_I is $u_{fI} = 0.00035$. At each position, substituting $n_g = 1.000\,2656$, $m = 43$–131, $u_{d_{FP}} = 0.065$ μm and $u_{f_I} = 0.000\,35$ into the equation (14) gives a combined standard uncertainty $u_L(k = 1) = 35.6$–35.9 μm and a combined expanded uncertainty (with coverage factor of $k = 2$) is $u_L(k = 2) = 71.2$–71.8 μm.

Because the value of m is not large, the contribution to measurement uncertainty of $u_{d_{FP}}$ is small. The main uncertainty contribution is u_{f_I}. Path length changes due to vibrations, uncertainty in the refractive index of air, the inaccuracy of resampling position and the intensity instability of the ECDL are the main reasons that result in the measurement uncertainty in the determination of f_I. If the sweeping range of the ECDL

was enlarged, more resampled points could be obtained and smaller measurement uncertainty could be obtained.

The residual error between the individual measurements done by FSI system and the fringe-counting interferometer is shown in figure 6. The central wavelength of the ECDL and the wavelength of the fringe-counting interferometer are both 633 nm so the refractive index is assumed to be to the same in their ranging formulas. The zero position is based on the average of 10 measurements. For each individual measurement, the agreement between the FSI system and the fringe-counting interferometer is within 100 μm. When averaged over 10 measurements, the largest difference is 28 μm. The standard deviation does not show a clear distance dependence and is on average 34 μm. Because environmental effects such as turbulence and vibrations will affect a single measurement result, averaging multiple measurements can improve the measurement accuracy and precision.

As mentioned above, arbitrary distances are chosen, but path length differences very close to $L_d = 0$ or $L_d = d_{FP}/4$ are avoided. At $L_d = 0$ m all wavelengths have the same phase (neglecting nonlinear air dispersion), so a typical cosine dependence like in figure 3 is not observed. Close to $L_d = d_{FP}/4$ the Nyquist frequency is approached and each period of the cosine is only determined by two points. In order to overcome the issue, a multiplex scheme could be envisaged. We can add another reference path to the measurement interferometer. By using a beam splitter and two shutters, then the reference path can be always selected such that the path length differences close to $L_d = 0$ m or $L_d = d_{FP}/4$ do not occur.

5. Conclusion

In this paper, we have proposed a method that substantially reduces the negative impacts of sweeping linearity, and absolute distance measurement result is obtained from the sparsely resampled signal. This method employs just one F–P cavity as the measurement reference to realize high accuracy arbitrary distance measurement. Compared to techniques using Mach–Zehnder interferometers, the F–P cavity is more stable and traceable. The F–P cavity being in vacuum, dispersion mismatch is avoided. Moreover, Hilbert transform algorithm and least square method are used to calculate the frequency of the resampled signal, which lead to an averaging effect in the analysis. Therefore, the influence of target vibration and other external random noise can be partially eliminated, and the reliability of the result is higher than a traditional FSI system. In the experiment, an ECDL with modulation range of 88GHz is used as the laser source. When compared with measurements done with a fringe-counting interferometer, the standard deviation of the residual errors is 34 μm. Sparsely resampling and smaller sweeping range are beneficial to reducing the processing cost and improving measurement efficiency. This method makes FSI system for absolute distance measurement more practical.

Funding

This work was supported by the National Natural Science Foundation of China under Grant No. 51505113; Zhejiang Provincial Natural Science Foundation of China under Grant No. LZ16E050001; and State Key Laboratory of Precision Measuring Technology and Instruments Project under Grant No. PIL1601.

ORCID iDs

Guang Shi https://orcid.org/0000-0002-3211-8105
Wen Wang https://orcid.org/0000-0002-0084-0910

References

[1] Muralikrishnan B, Phillips S and Sawyer D 2016 Laser trackers for large-scale dimensional metrology: a review *Precis. Eng.* **44** 13–28
[2] Coddington I, Swann W C, Nenadovic L and Newbury N R 2009 Rapid and precise absolute distance measurements at long range *Nat. Photon.* **3** 351–6
[3] Komissarov R, Kozlov V, Filonov D and Ginzburg P 2019 Partially coherent radar unties range resolution from bandwidth limitations *Nat. Commun.* **10** 1423
[4] Yang R, Pollingerl F, Meiners-Hagen K, Krystekl M, Tan J and Bossel H 2015 Absolute distance measurement by dual-comb interferometry with multi-channel digital lock-in phase detection *Meas. Sci. Technol.* **26** 084001
[5] Guillory J, de la Serve M T, Truong D, Alexandre C and Wallerand J 2019 Uncertainty assessment of optical distance measurements at micrometer level accuracy for long-range applications *IEEE Trans. Instrum. Meas.* **68** 2260–7
[6] Liu Z, Liu Z, Deng Z and Tao L 2016 Interference signal frequency tracking for extracting phase in frequency scanning interferometry using an extended Kalman filter *Appl. Opt.* **55** 2985–92
[7] Medhat M, Sobee M, Hussein H and Terra O 2016 Distance measurement using frequency scanning interferometry with mode-hoped laser *Opt. Laser Technol.* **80** 209–13
[8] DiLazaro T and Nehmetallah G 2018 Large-volume, low-cost, high-precision FMCW tomography using stitched DFBs *Opt. Express* **26** 2891–904
[9] Cabral A P and Rebordão J M 2007 Accuracy of frequency-sweeping interferometry for absolute distance metrology *Opt. Eng.* **46** 073602
[10] Cabral A P and Rebordão J M 2010 Dual-frequency sweeping interferometry for absolute metrology of long distances *Opt. Eng.* **49** 5601
[11] Jia X, Liu Z, Tao L and Deng Z 2017 Frequency-scanning interferometry using a time-varying Kalman filter for dynamic tracking measurements *Opt. Express* **25** 25782–96
[12] Tao L, Liu Z, Zhang W and Zhou Y 2014 Frequency-scanning interferometry for dynamic absolute distance measurement using Kalman filter *Opt. Lett.* **39** 6997–7000
[13] Jia X, Liu Z, Deng Z, Deng W, Wang Z and Zhen Z 2018 Dynamic absolute distance measurement by frequency

sweeping interferometry based Doppler beat frequency tracking model *Opt. Commun.* **430** 163–9
[14] Deng Z, Liu Z, Li B and Liu Z 2015 Precision improvement in frequency-scanning interferometry based on suppressing nonlinear optical frequency sweeping *Opt. Rev.* **22** 724–30
[15] Baumann E, Giorgetta F R, Coddington I, Sinclair L C, Knabe K, Swann W C and Newbury N R 2013 Comb-calibrated frequency-modulated continuous-wave ladar for absolute distance measurements *Opt. Lett.* **38** 2026–8
[16] Baumann E, Giorgetta F R, Deschênes J-D, Swann W C, Coddington I and Newbury N R 2014 Comb-calibrated laser ranging for three-dimensional surface profiling with micrometer-level precision at a distance *Opt. Express* **22** 24914–28
[17] Hariyama T, Sandborn P A, Watanabe M and Wu M C 2018 High-accuracy range-sensing system based on FMCW using low-cost VCSEL *Opt. Express* **26** 9285–97
[18] Pan H, Zhang F, Shi C and Qu X 2017 High-precision frequency estimation for frequency modulated continuous wave laser ranging using the multiple signal classification method *Appl. Opt.* **56** 6956–61
[19] Lu C, Liu G, Liu B, Chen F and Gan Y 2016 Absolute distance measurement system with micron-grade measurement uncertainty and 24 m range using frequency scanning interferometry with compensation of environmental vibration *Opt. Express* **24** 30215–24
[20] Tao L, Liu Z, Zhang W, Liu Z and Hong J 2017 Real-time drift error compensation in a self-reference frequency-scanning fiber interferometer *Opt. Commun.* **382** 99–104
[21] Pan H, Qu X and Zhang F 2018 Micron-precision measurement using a combined frequency-modulated continuous wave ladar autofocusing system at 60 m standoff distance *Opt. Express* **26** 15186–98
[22] Guodong L, Xinke X, Bingguo L, Fengdong C, Tao H, Cheng L and Yu G 2017 Dispersion compensation method based on focus definition evaluation functions for high-resolution laser frequency scanning interference measurement *Opt. Commun.* **386** 57–64
[23] Van Den Berg S A, Van Eldik S and Bhattacharya N 2015 Mode-resolved frequency comb interferometry for high-accuracy long distance measurement *Sci. Rep.* **5** 14661
[24] Van den Berg S, Persijn S, Kok G, Zeitouny M and Bhattacharya N 2012 Many-wavelength interferometry with thousands of lasers for absolute distance measurement *Phys. Rev. Lett.* **108** 183901
[25] Lešundák A, Voigt D, Cip O and van den Berg S 2017 High-accuracy long distance measurements with a mode-filtered frequency comb *Opt. Express* **25** 32570–80
[26] Joint Committee for Guides in Metrology 2008 *Evaluation of Measurement Data—Guide to the Expression of Uncertainty in Measurement (Bureau International des Poids et Mesures (BIPM))* (www.bipm.org/utils/common/documents/jcgm/JCGM_100_2008_E.pdf)